

Effective Modeling for Coarse Grained Simulations of Shock Driven Turbulent Mixing

F.F. Grinstein, J.A. Saenz, R.M. Rauenzahn, and M.M. Francois
Corresponding author: fgrinstein@lanl.gov; LA-UR-18-24694

Los Alamos National Laboratory, Los Alamos, NM 87545, USA.

Abstract: We focus on simulating the consequences of material interpenetration, hydrodynamical instabilities, and mixing arising from perturbations at shocked material interfaces, as vorticity is introduced by the impulsive loading of shock waves – e.g., as in ICF capsule implosions. In the coarse grained simulation (CGS) paradigm small scales are presumed enslaved to the dynamics of the largest, or put in other words, the spectral cascade rate of energy (*the rate limiting step*) is determined by the initial and boundary condition constrained large-scale dynamics. CGS includes classical large-eddy simulation (LES) using explicit subgrid scale (SGS) models, and implicit LES (ILES) relying on SGS modeling implicitly provided by physics capturing numerics. By combining shock and turbulence emulation capabilities based on a single (physics capturing) numerics, ILES provides an effective simulation framework for shock driven turbulent mixing. Beyond the complex multiscale resolution issues of shocks and variable density turbulence, we must address the difficult problem of predicting flow transition promoted by energy deposited at the material interfacial layer during the shock interface interactions. Transition involves unsteady large-scale coherent-structure dynamics capturable by CGS but not by an unsteady Reynolds-Averaged Navier-Stokes (RANS) approach based on single-point-closure modeling. We discuss a dynamic blended hybrid RANS/ILES strategy for applications involving variable-density turbulent mixing applications, and report progress testing their preliminary implementation for relevant canonical problems.

Keywords: shock driven turbulence, large eddy simulation.

1 Introduction

Simulations of unsteady shock-driven turbulent mixing flows are typically required to capture late-time states of complex, convectively-driven multi-physics in applications of programmatic interest, such as inertial confinement fusion (ICF) capsule implosions. The three-dimensional (3D) hydrodynamics depends on initial conditions (IC) and involves transition to turbulence, non-equilibrium turbulence development and decay, and relaminarization. Such flow physics can be captured with coarse-grained simulation (CGS) [1], presuming small-scale flow-dynamics are enslaved to dynamics of the largest scales, and using mixing transition criteria for macroscopic convergence metrics [2].

CGS includes classical large-eddy simulation (LES) using explicit subgrid scale (SGS) models, and implicit LES (ILES) [3] relying on SGS modeling implicitly provided by *physics-capturing* numerics. Classical explicit SGS models are comparable to their implicit counterparts provided by the numerics in the standard LES practice [4, 5], motivating ILES for high Reynolds-number (Re) shock-driven and convectively-driven turbulent mixing [1]. Depending on Re , Schmidt and Damkohler numbers, mixed explicit/implicit SGS models are used for non-convective physics such as backscatter, diffusive mixing, and combustion.

Late-time states depend on IC. Because of IC uncertainties [6], ensemble averaging deterministic CGS over a suitably complete set of realizations covering the relevant IC variability is often a strategy of choice – albeit computationally expensive for most 3D turbulent flows of practical interest. We propose to capture relevant aspects of the flow transition physics using hybrid approaches blending CGS and Reynolds-Averaged

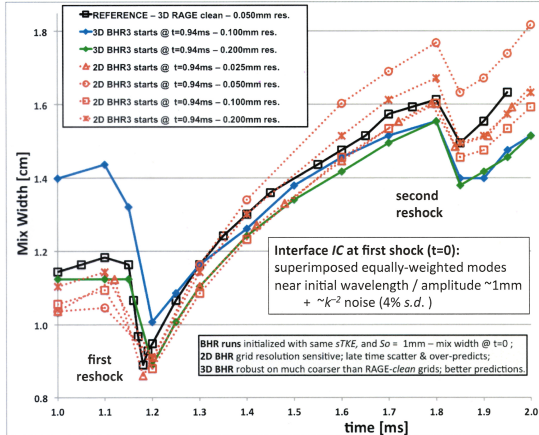


Figure 1: Sequential ILES/RANS simulations [9]: RANS is initialized with ILES flow data at $t=0.94\text{ms}$ just before 1st reshock. Coarse grid 3D RANS is robust and accurate between 1st and 2nd reshock. 2D RANS tend to be more sensitive to their IC (at start time) and grid resolution compared with their 3D counterparts; scatter of the 2D results is more pronounced near the new transitional flow event at second reshock as we move out from near equilibrium flow conditions.

Navier-Stokes (RANS) models [7] – which we envision as a computationally feasible method to represent ensemble averaging while also addressing the additional degrees of freedom associated with transition and small-scale dynamics.

2 Problem Statement

A prototypical laboratory shock-tube experiment of interest for ICF involves transitional non-equilibrium flow at first-shocked and subsequently reshocked (initially-perturbed) material interfaces, relaxing to quasi-equilibrium decaying turbulence between shock events. Transition can be captured by ILES, but not by RANS based on single-point-closure modeling [8]. However, RANS on coarser grids – and often reduced dimension (1D and 2D) – are preferred for engineering and design purposes. RANS are generally based on slaving enstrophy production to kinetic energy production and to equilibrium turbulence paradigms. There are outstanding problems in using such RANS for shock-driven turbulence: 1) transitional IC-dependent flow physics is 3D and non-equilibrium; 2) mechanisms for enstrophy generation are inherently very different from those underlying energy production.

Notwithstanding its shortcomings, RANS can be effectively used following each transitional event with suitable initialization. In [9] *sequential* CGS/RANS hybrid simulation studies were reported for the CEA shock tube experiments [10], in which ILES-generated data provided physics-based IC to RANS and was also used as reference for its assessment. We compared state-of-the-art ILES and 3D RANS using the xRAGE code [11] in the ILES (“clean”) and RANS (“BHR”) versions [13] (e.g., Figure 1 from [9]). We found that by prescribing ILES generated 3D IC and allowing for 3D convection with just enough resolution, the computed dissipation in 3D RANS (vs. 2D RANS) effectively supplements the modeled dissipation – rather than multiple-counting developed-turbulence effects. However, RANS cannot capture well the consequences of a new subsequent transitional flow event (e.g., 2nd reshock in Figure 1) – where activating CGS again in some fashion would appear useful. We here propose that the *sequential* hybrid be continued with a *blended* hybrid ILES/RANS strategy [7] – the flow simulation methodology (FSM) (e.g. [14]), and report progress extending formalism and implementation for the variable-density compressible regimes of interest in shock-driven turbulent mixing.

It is important to note here that BHR is a RANS simulation approach, and as such it is theoretically justified and derived to model ensemble flows in which space and time turbulent fluctuations are removed by the ensemble average. BHR is thus designed to provide ensemble-averaged turbulent quantities and to be used at relatively coarse resolutions in which prognostic variables are ensemble-averaged, mean flow quantities. This presents a potential challenge as we mix ILES and BHR for intermediate-to-fine resolutions, where a suitable blended hybrid implementation may need to be appropriately constrained to ensure that spurious small-scale contributions from BHR are minimized.

FSM locally blends a high resolution computational strategy with RANS modeling – depending on how much of the turbulence is resolved at given resolution, providing a sophisticated CGS strategy in-between. How much dissipation is modeled and how much is computed is decided based on having the

RANS model locally morph into a CGS SGS model, $\tau_{ij}^{CGS} = f(\Delta/L)\tau_{ij}^{RANS}$, where the contribution function $0 < f(\Delta/L) < 1$ is 0 at the high resolution limit – involving here ILES, and 1 at the low resolution limit (pure RANS), Δ is the local grid size, and L is a physical resolution scale. We use strategy proposed by Germano [15] to generate f dynamically, by using an identity relating total, unresolved and resolved stresses, and a differential filter as secondary filtering operation [16]. We report our progress developing and testing our dynamic blended hybrid ILES/RANS.

3 Blended Hybrid LES / RANS

Standards for industrial aerospace and automotive simulations rely on 3D hybrid LES/URANS to drastically reduce computational costs in full-scale configurations. Hybrid LES/RANS strategies exploit the structural similarity between equations for computed RANS and LES velocity solutions [7]. Historically, two classes of hybrid LES/RANS have been considered: zonal and blended. In the zonal approaches, a clear distinction is made between near-wall (RANS) and detached flow (LES) regions, the most widely used zonal hybrid being *detached eddy simulation*, (DES) [17]. With blended hybrid LES/RANS – our focus here – a continuous application is sought, in which a single turbulence model locally adjusted based on local resolution is used.

The flow simulation methodology (FSM) proposed by Speziale [18] and subsequently pursued in various forms by others – e.g., [14, 19, 20, 21], seeks to locally blend direct numerical simulations (DNS) and RANS as function of grid resolution, effectively providing a sophisticated LES strategy in-between. How much dissipation is modeled and how much is computed is decided based on having the RANS model locally morph into LES SGS model, in terms of the contribution factor $0 < f(\Delta/L) < 1$ introduced above. The role of the contribution factor is to damp the contribution of the RANS model, as part of the unsteady turbulence becomes resolved in the intermediate (LES) regime. The issue of interest is the computation of the dissipation which, when under-resolved, has to be complemented by the model in the hybrid context. For sufficiently fine resolution the entire dissipation range is resolved and the RANS contribution should switch itself off –i.e., $f(\Delta/L_k) \rightarrow 0$ as $\Delta \rightarrow 0$. Hence, the original idea in [18] to estimate the *distance to DNS* by computing the factor Δ/L_k with L_k being a Kolmogorov length estimate based on the RANS computed dissipation.

In [18, 14] a contribution function was proposed on a phenomenological basis of the following form,

$$f(\Delta/L) = [1 - \exp(-\beta\Delta/L_k)]^n$$

using $\beta = 0.001$ and $n = 1$, where n controls the steepness of the function and β effectively determines at what grid resolution the model contribution becomes negligible. Such contribution factors are typically used for compressible aerospace applications [14]. Similarly, another proposal [19] used,

$$f(\Delta/L) = [1 - \exp(-\beta'\Delta^2)]^m$$

without reference to a physical length-scale but still retaining *ad hoc* parameters β' and m , whereas the proposal in [20] was,

$$f(\Delta/L) = \nu_{LES}/\nu_{RANS} \sim \Delta^2/S^2$$

where ν_{RANS} denotes eddy viscosity, S is a turbulent length scale (both RANS computed), and $\nu_{LES} \sim \Delta^2$ is typical choice for a Smagorinsky LES SGS model.

As defined above, local grid resolution effectively defines the contribution factor locally driven by eventual adaptive mesh refinement (AMR) design specifics and/or researcher-provided resolution requirements (customarily based on physical and empirical insights). Ideally, LES is Navier-Stokes (NS) based and the smallest resolved length scale is fixed by a characteristic (grid independent) filter length [23]. However, results are still dependent on the filter-length chosen. Most typically, well established practical LES relies on filtering provided by the grid – e.g., [24], and competition between explicit SGS modeling and filtering and their counterparts provided by the numerics raise seemingly insurmountable issues for under-resolved systems [5] – which has historically motivated ILES [3]. LES models generated through the blended LES/RANS hybrids cited above are also grid (or filter length) dependent.

With empirical aspects on AMR design/use for the problems of practical interest being unavoidable, small-scale resolution issues need to be carefully addressed and suitably incorporated in hybrid LES/RANS validation and uncertainty quantification metrics. In what follows, we consider implicit dependence of the contribution function on grid size Δ in the context of a *dynamic* blended hybrid strategy. This is in contrast with the classical blended hybrid strategies above defining the contribution functions explicitly in terms of local Δ in fairly *ad hoc* fashion,

4 xRAGE-BHR Blended Hybrid Governing Equations

Turbulent mixing of material scalars can be usefully characterized by the length scales of the fluid physics involved: 1) large-scale entrainment in which advection brings relatively large regions of the pure materials together, 2) an intermediate length scale associated with the convective stirring due to velocity gradient fluctuations, and, 3) much smaller scale interpenetration resulting from molecular diffusion. Large-scale vortices and their interactions play a crucial role in controlling transitional growth and entrainment at moderately high Re – when convective time-scales are much smaller than those associated with molecular diffusion. In this limit, the primary concern is with the numerical simulation of the first two processes above – advection and stirring. Both Navier-Stokes and Euler based ILES are capable of capturing high-Re-dominating stirring (convectively) driven mixing.

We consider here an ILES strategy based on the Radiation Adaptive Grid Eulerian (xRAGE) code; xRAGE solves the multi-material compressible conservation equations for mass density ρ , material concentrations Y_n , momenta ρu_i and , total energy E [11] – equations immediately following below with $f = 0$, with spatial-filtering (*overbars*) and Favrè- averaging (*tildes*) reducing to grid-filtered and simply-scaled values, respectively. We use the Besnard-Harlow-Rauenzahn (BHR) multi-equation RANS framework [25] to include the effects of turbulence development in the presence of density and pressure gradients, based on ensemble-averaging the said equations, which results in a new set of equations for the flow variables and material concentrations – the equations below with $f = 1$, including closure models and additional transport equations for the turbulent turbulence length scale, turbulent mass fluxes, density-specific-volume covariance, and Reynolds stress transport. See recent BHR references [26, 27, 13] for more details. For now, we conveniently use the contribution function f as a formal place-holder scaling factor – to be revisited further below when discussing blended hybrid strategies in the xRAGE context. Beyond the formal introduction of f for the Reynolds stress terms in incompressible flow equations in [18], we have extended the use by [14] for the compressible flow case, now also allowing for multiple-species variable density regimes.

The governing equations for the mean flow are modified by scaling the turbulence model terms by the contribution function f , as follows,

$$\frac{\partial \bar{\rho}}{\partial t} + (\bar{\rho} \tilde{u}_j)_{,j} = 0 \quad (1)$$

$$\frac{\partial \bar{\rho} \tilde{Y}_n}{\partial t} + (\bar{\rho} \tilde{u}_j \tilde{Y}_n)_{,j} = \left(C_c \frac{S}{\sqrt{K}} \bar{\rho} f \tilde{R}_{jm} \tilde{Y}_{n,m} \right)_{,j} \quad (2)$$

$$\frac{\partial \bar{\rho} \tilde{u}_i}{\partial t} + (\bar{\rho} \tilde{u}_i \tilde{u}_j + \bar{P} \delta_{ij})_{,j} + V.T. = - \left(\bar{\rho} f \tilde{R}_{ij} \right)_{,j} + \bar{\rho} g_i \quad (3)$$

$$\begin{aligned} \frac{\partial \bar{\rho} \tilde{E}}{\partial t} &+ \left(\bar{\rho} \tilde{u}_j \tilde{E} + \bar{P} \tilde{u}_j \right)_{,j} + V.T. = \\ &- \left(\bar{\rho} f \tilde{u}_i \tilde{R}_{ij} \right)_{,j} + \left[\bar{\rho} f \tilde{R}_{ij} \frac{S}{\sqrt{K}} \left(C_k K_{,j} + C_e \frac{C_\nu}{P_{r_t}} \tilde{T}_{,j} + C_c \bar{h}^n \tilde{Y}_{n,j} \right) \right] \end{aligned} \quad (4)$$

In the above, the Favrè-averaged Reynolds stress is defined as

$$\tilde{R}_{ij} = \frac{\overline{\rho u_i'' u_j''}}{\bar{\rho}} \quad (5)$$

and the turbulent kinetic energy is

$$K = \frac{R_{ii}}{2}, \quad (6)$$

$V.T.$ in the momenta and energy equations denotes mixture viscous terms. The above equations are supplemented with appropriate equations of state. The closure equations are given by the second-moment closure BHR model and are not modified in our formulation. For more details, refer to [26, 27, 13]. The closure equations are given by

$$\begin{aligned} \frac{\partial \bar{\rho} \tilde{R}_{ij}}{\partial t} + (\bar{\rho} \tilde{u}_k \tilde{R}_{ij})_{,k} &= (1 - C_{r1})[a_i \bar{P}_{,j} + a_j \bar{P}_{,i}] + \bar{\rho}(C_{r2} - 1)[\tilde{R}_{ik} \tilde{u}_{j,k} + \tilde{R}_{jk} \tilde{u}_{i,k}] \\ &+ C_r \left(\frac{S}{\sqrt{K}} \bar{\rho} \tilde{R}_{kn} \tilde{R}_{ij,n} \right)_{,k} - C_{r3} \bar{\rho} \frac{\sqrt{K}}{S} (\tilde{R}_{ij} - \frac{1}{3} \tilde{R}_{kk} \delta_{ij}) \\ &- C_{r2} \frac{2}{3} \bar{\rho} \tilde{R}_{mk} \tilde{u}_{m,k} \delta_{ij} + C_{r1} \frac{2}{3} a_k \bar{P}_{,k} \delta_{ij} - \bar{\rho} \frac{2}{3} \frac{K \sqrt{K}}{S} \delta_{ij} \end{aligned} \quad (7)$$

$$\begin{aligned} \frac{\partial \bar{\rho} S}{\partial t} + (\bar{\rho} \tilde{u}_j S)_{,j} &= -\frac{S}{K} \left(\frac{3}{2} - C_1 \right) \bar{\rho} \tilde{R}_{ij} \tilde{u}_{i,j} + C_S \left(\frac{S}{\sqrt{K}} \bar{\rho} \tilde{R}_{kn} S_{,n} \right)_{,k} \\ &- \left(\frac{3}{2} - C_2 \right) \rho \sqrt{K} + \frac{S}{K} \left(\frac{3}{2} - C_3 \right) a_j \bar{P}_{,j} - C_4 \bar{\rho} S \bar{u}_{j,j} \end{aligned} \quad (8)$$

$$\begin{aligned} \frac{\partial \bar{\rho} a_i}{\partial t} + (\bar{\rho} \tilde{u}_k a_i)_{,k} &= b \bar{P}_{,i} - \tilde{R}_{ik} \bar{\rho}_{,k} - \bar{\rho} a_k (\tilde{u}_i - a_i)_{,k} + \bar{\rho} (a_k a_k)_{,k} \\ &+ \bar{\rho} C_a \left(\frac{S}{\sqrt{K}} \tilde{R}_{kn} a_{i,n} \right)_{,k} - C_{a1} \bar{\rho} \frac{\sqrt{K}}{S} a_i \end{aligned} \quad (9)$$

$$\frac{\partial \bar{\rho} b}{\partial t} + (\bar{\rho} \tilde{u}_k b)_{,k} = -2(b+1) a_k \bar{\rho}_{,k} + 2 \bar{\rho} a_k b_{,k} + \bar{\rho}^2 C_b \left(\frac{S}{\rho \sqrt{K}} \tilde{R}_{mn} b_{,n} \right)_{,m} - C_{b1} \bar{\rho} \frac{\sqrt{K}}{S} b \quad (10)$$

In addition to the primary flow variables, the TKE, turbulent length scale, turbulent mass flux, Reynolds stress, and density-specific-volume covariance must be initialized [13]. The established BHR running procedures initialize the specific TKE, turbulent length scale, and turbulent mass flux with suitable uniformly distributed prescribed constant values. Ideally, the turbulence intensity should be zero, however, this initialization is difficult to implement numerically and therefore it is customary to start with a reasonably low non-zero value. The diagonal components of the Reynolds stress tensor are initialized as isotropic and the off diagonal components are initialized to zero. The initial turbulent length scale is based on material interface characteristics such as surface perturbations or surface finish. The initial turbulent mass fluxes are set to zero. The initial density-specific-volume covariance is set to characteristic two-fluid unmixed values representing the least mixed extrema of the field for the material configuration of interest.

Depending on the system of equations xRAGE-BHR falls back to in the high-resolution limit ($f = 0$), there are two different blended hybrids to be considered. Firstly, we consider the high-Re limit with negligible viscosity effects ($V.T. = 0$), and we have xRAGE-BHR falling back to nominally-inviscid Euler-based xRAGE ILES for ($f = 0$). In this case, a useful local physical resolution reference length-scale can be a user-provided Taylor-microscale length estimate. Otherwise, when viscosity effects are not negligible, NS-based xRAGE ILES is correspondingly generated, and we may need a viscous resolution length scale such as an estimated Kolmogorov length scale [18].

5 A Dynamic Contribution Function

Our approach to finding a contribution function f [18, 14] for variable density turbulence simulations using BHR [25, 26] is largely based on [15]. Define the Favre average of a quantity q as

$$\tilde{q} = \frac{\langle \rho q \rangle}{\langle \rho \rangle}. \quad (11)$$

The Favre averaged Reynolds stress in BHR, equation (7), $R_{ij}^{RANS} \equiv \tilde{R}_{ij}$, is

$$R_{ij}^{RANS} = \frac{\langle \rho u_i'' u_j'' \rangle}{\langle \rho \rangle}, \quad (12)$$

or

$$R_{ij}^{RANS} = \frac{\langle \rho u_i u_j \rangle}{\langle \rho \rangle} - \tilde{u}_i \tilde{u}_j. \quad (13)$$

where $\langle \cdot \rangle$ is an ensemble average in the RANS sense, or an average in a subspace of statistical homogeneity in a space - time domain.

Define the analogue to the Favre average at the SGS, or SGS Favre average, of a quantity q as

$$\hat{q} = \frac{\overline{\rho q}}{\bar{\rho}}. \quad (14)$$

where the overbar $\overline{\cdot\cdot\cdot}$ denotes an implicit grid filter, and e.g. \hat{u}_i is the resolved velocity in a simulation at a given resolution. Using this filter we can obtain an expression for the SGS, or un-resolved, Favre averaged Reynolds stress,

$$R_{ij}^s = \frac{\overline{\rho u_i u_j}}{\bar{\rho}} - \hat{u}_i \hat{u}_j. \quad (15)$$

To derive an expression for the total stress, multiply (15) by $\bar{\rho}$, and average to obtain

$$\langle \bar{\rho} R_{ij}^s \rangle = \langle \overline{\rho u_i u_j} \rangle - \langle \bar{\rho} \hat{u}_i \hat{u}_j \rangle, \quad (16)$$

from which we solve for

$$\langle \rho u_i u_j \rangle = \langle \bar{\rho} R_{ij}^s \rangle + \langle \bar{\rho} \hat{u}_i \hat{u}_j \rangle, \quad (17)$$

where we have assumed statistical consistency of the LES [22], i.e.

$$\langle \overline{\cdot\cdot\cdot} \rangle = \langle \cdot\cdot\cdot \rangle. \quad (18)$$

Note that in [22], statistical consistency is enforced to derive a dynamic Smagorinsky coefficient, while here we assume statistical consistency and heavily rely on 18. We will discuss this more later.

Replace (17) in (13), to obtain

$$R_{ij}^{RANS} = \frac{\langle \bar{\rho} R_{ij}^s \rangle}{\langle \bar{\rho} \rangle} + \frac{\langle \bar{\rho} \hat{u}_i \hat{u}_j \rangle}{\langle \bar{\rho} \rangle} - \frac{\langle \bar{\rho} \hat{u}_i \rangle}{\langle \bar{\rho} \rangle} \frac{\langle \bar{\rho} \hat{u}_j \rangle}{\langle \bar{\rho} \rangle}. \quad (19)$$

Define the resolved Favre averaged stress as

$$T_{ij} = \frac{\langle \bar{\rho} \hat{u}_i \hat{u}_j \rangle}{\langle \bar{\rho} \rangle} - \frac{\langle \bar{\rho} \hat{u}_i \rangle}{\langle \bar{\rho} \rangle} \frac{\langle \bar{\rho} \hat{u}_j \rangle}{\langle \bar{\rho} \rangle}, \quad (20)$$

and the SGS-Favre average of the SGS stress as

$$\tilde{R}_{ij}^s = \frac{\langle \bar{\rho} R_{ij}^s \rangle}{\langle \bar{\rho} \rangle} \quad (21)$$

and the total stress becomes

$$R_{ij}^{RANS} = \tilde{R}_{ij}^s + T_{ij}. \quad (22)$$

Equation (22) is the form that the Germano identity takes in variable density turbulent flows. It states that the total Favre averaged Reynolds stress R_{ij}^{RANS} is equal to the sum of the Favre averaged SGS stress and the resolved stress.

We make the following assumptions:

- The RANS stress is equal to a RANS model stress, $R_{ij}^{RANS} = R_{ij}^m$, and in general, RANS tensor quantities are equal to RANS model quantities. In other words, we rely on the the model providing an accurate estimate of the RANS quantities it represents.
- **We assume that the RANS model can be used as a function of resolved variables in the LES context – where eddies are permitted, to represent RANS quantities.** The formulation of the dynamic contribution function relies on $R_{ij}^{RANS} = R_{ij}^m$, i.e. it relies on the model Reynolds stress accurately representing the total Reynolds stress. RANS models are derived to do this by representing the physics of closure terms as a function of the mean flow in ensemble averaged flows, where eddies are averaged out. Calculating the RANS model stress R_{ij}^m as a function of the resolved flow in a LES where there are eddies may very well not provide an accurate estimate of the total (RANS) Reynolds stress. Previous attempts to use a similar hybrid formulation [28] reported use of R_{ij}^m as a function of (time) filtered resolved flow variables for this reason.
- We will interpret \tilde{R}_{ij}^s as the hybrid model stress R_{ij}^h that we are after, which can be a combination of an LES SGS model stress and a RANS closure model stress, as in [29, 28].
- $\langle \overline{\cdot \cdot \cdot} \rangle = \langle \cdot \cdot \cdot \rangle$, which is a requirement if we want to smoothly transition from LES to RANS.
- In our context, $\hat{q} = \tilde{q}$ is a primitive variable in the resolved flow.

With these assumptions we have,

$$R_{ij}^m = R_{ij}^h + T_{ij}. \quad (23)$$

We use ILES as high-resolution limit strategy, so there is no explicit LES SGS model. In this way, the hybrid stress is related to the RANS model stress by

$$R_{ij}^h = f(\Delta/L) R_{ij}^m \quad (24)$$

where we expect the contribution function $f = 0$ at the high resolution limit (pure ILES), and $f = 1$ at the low resolution limit (pure RANS), $0 \leq f(\Delta/L) \leq 1$.

We substitute equation (24) into (23), take the scalar product with a RANS tensor quantity q_{ij}^m , and solve for the contribution function to get

$$f(\Delta/L) = 1 - \frac{q_{ij}^m T_{ij}}{q_{ij}^m R_{ij}^m}. \quad (25)$$

In the original formulation in [15], the RANS model Reynolds stress is used, $q_{ij}^m = \tau_{ij}^m$, while [29, 28] use the RANS model strain rate, $q_{ij}^m = S_{ij}^m$.

In our approach, the filter $\langle \cdot \rangle$ corresponds to a Helmholtz differential filter [16, 30],

$$\hat{q} = \langle q \rangle - \nabla \cdot \frac{\Delta^2}{c} \nabla \langle q \rangle. \quad (26)$$

To evaluate the behavior of the dynamic contribution function derived in this section, we diagnose the turbulent kinetic energy (TKE). We take the trace of the total stress in (22), after replacing the expression for the hybrid SGS in equation (24), to obtain

$$K^T = K^u + K^r, \quad (27)$$

where K^T is the total turbulent kinetic energy, $K^u = fK^m$ is the unresolved or SGS (modeled) turbulent kinetic energy, K^m is turbulent kinetic energy from the BHR model, and K^r is the resolved turbulent kinetic energy. Given the expected behavior of f , K^T will be dominated by the resolved K^r at high resolution simulations with small grid size, while at low resolution, large grid size, K^T will be dominated by the modeled (unresolved) K^u . Thus, as resolution decreases, the simulation relies more on BHR.

6 The Taylor-Green Vortex

The TGV has been used as prototype for vortex stretching, instability and production of small-scale eddies to examine the dynamics of transition to turbulence based on DNS [31]. The DNS of Brachet et al. [31], was based on the solution of the incompressible NS equations using spectral methods, and exploited the spatial symmetries of the TGV to reduce the effective computational cost by a factor of 8. The simulations were originally performed on a grid of 256^3 modes in 1983 [31] – to resolve Re up to $Re = 3000$, and repeated with 864^3 modes nearly a decade later [32] – to resolve $Re = 5000$. The TGV case has also been used to demonstrate how the convective numerical diffusion of certain algorithms can be used to emulate the dominant SGS physics of transition to turbulence for high (but-finite) Re flows [33].

The TGV configuration considered here involves triple-periodic boundary conditions enforced on a cubical domain with box side length 2π cm using evenly spaced computational cells. The flow is initialized with the solenoidal velocity components,

$$\begin{aligned} u &= U_o \sin(k_o x) \cos(k_o y) \cos(k_o z), \\ v &= -U_o \cos(k_o x) \sin(k_o y) \cos(k_o z), \\ w &= 0, \end{aligned}$$

and the pressure given by a solution of the Poisson equation for the above given velocity field, i.e.,

$$p = p_o + (\rho U_o^2 / 16) [2 + \cos(2k_o z)] [\cos(2k_o x) + \cos(2k_o y)],$$

where we further select $p_o = 1.0$ bar, mass density, $\rho = 1.178 \text{ kg/m}^3$, $U_o = 100 \text{ m/s}$ and an ideal gas equation of state for air (corresponding to low Ma , $Ma = 0.28$). Convenient non-dimensional units are $t^* = k_o U_o t$, $x^* = k_o x$; $k_o = 1$ was selected.

For the present TGV analysis the kinetic dissipation rate $-dK^*/dt^*$ involves the non-dimensionalized volumetric mean integrated kinetic energy:

$$K = \frac{1}{2} \frac{\langle \rho u_i u_i \rangle}{\langle \rho \rangle}, \quad (28)$$

where the operator $\langle \rangle$ is defined for a generic quantity q as

$$\langle q \rangle = \frac{1}{V} \int q \, dx dy dz. \quad (29)$$

The TGV mean enstrophy can be defined by:

$$\Omega = \langle \omega_i \omega_i \rangle. \quad (30)$$

Asymptotic equilibrium (Re independent) dissipation is suggested by Brachet's TGV kinetic energy dissipation results included in Figure 2 [31, 32]. The DNS data in Figure 2 shows consistent dissipation peaks near $t^* \sim 9$, for $Re=800, 1600, 3000$, and 5000 , and the almost indistinguishable results for $Re=3000$ and 5000 suggest that they may be close to a viscosity independent limit [35]. Whether or not this finite-time singularity exists for the purely inviscid case remains unsettled and controversial [36]. Characteristic times at dissipation peaks (as well as wider peaks) are predicted by the DNS results as Re is lowered.

Instantaneous visualizations of the TGV flow dynamics (from [33]) are shown in Figure 3. The snapshots are based on ray-tracing volume renderings of λ_2 – the second-largest eigenvalue of the velocity gradient tensor [34]. The images display the initial transition to increasingly smaller-scale (organized) vortices and

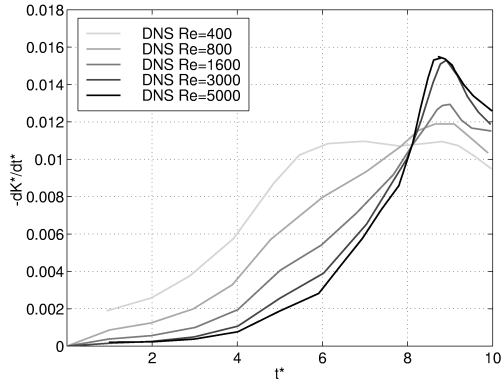


Figure 2: Taylor-Green vortex kinetic energy dissipation rate from DNS [31, 32].

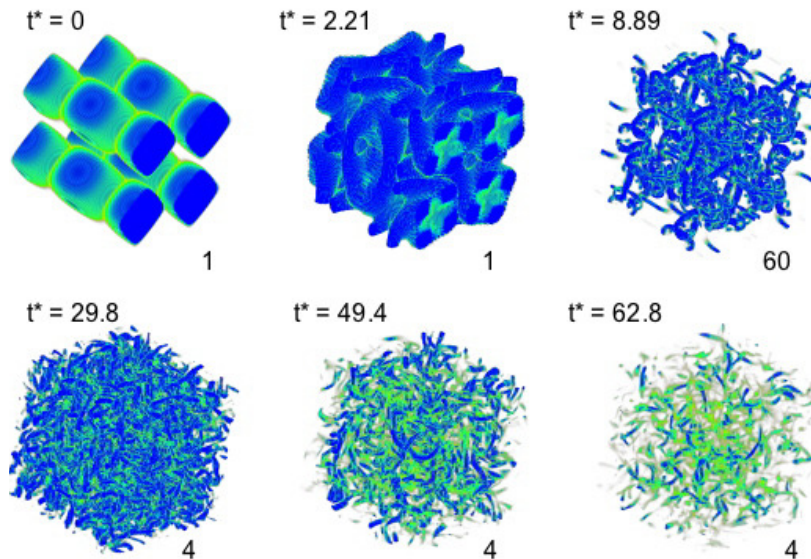


Figure 3: Instantaneous TGV visualizations in terms of volume renderings of λ_2 ; hue and opacity maps are the same for all times; peak vorticity magnitude values (normalized by value at $t^*=0$) are indicated at the lower right of each frame.

then to the fully developed (disorganized) decaying worm-vortex dominated flow regime characteristic of developed turbulence. The fastest decay rate at the dissipation peak (at $t^* \sim 9$) in Figure 2 depicts the onset of the inviscid TGV instability and is also associated with peak enstrophy.

CGS strategies have been verified in the TGV context, for a wide range of classical LES and ILES [33]. The mathematical flow simulation model was based on the conservation equations of mass, momentum, and energy. ILES models tested in [33] examined Euler based nominally inviscid flow (as considered here) or NS based linear viscous flow. Results of the TGV studies indicated that a Re independent regime is asymptotically attained with ILES with increasing grid resolution. The observation of earlier transition times of the dissipation peaks, as well as lower and wider peaks, were predicted by the coarser-grid ILES, a trend consistently exhibited by the DNS results as the Re is lowered. We also found a consistent correlation between non-dimensional profiles of mean kinetic energy dissipation rates and mean enstrophy Ω [33, 37]. Peak mean enstrophy values increase with grid resolution, and the correlation between mean kinetic energy dissipation and mean enstrophy expected for an incompressible NS fluid with Reynolds number Re is effectively satisfied – reflecting on the unsteady physical dissipation being captured with ILES.

We use xRAGE to run simulations on uniform resolution meshes with a total number of points of $N^3 = 32^3, 64^3, 128^3$, and 256^3 , respectively. For each case, the initial turbulent length scale in BHR is initialized at the grid size of the corresponding mesh, $S_o = \Delta$. The initial BHR specific turbulent kinetic

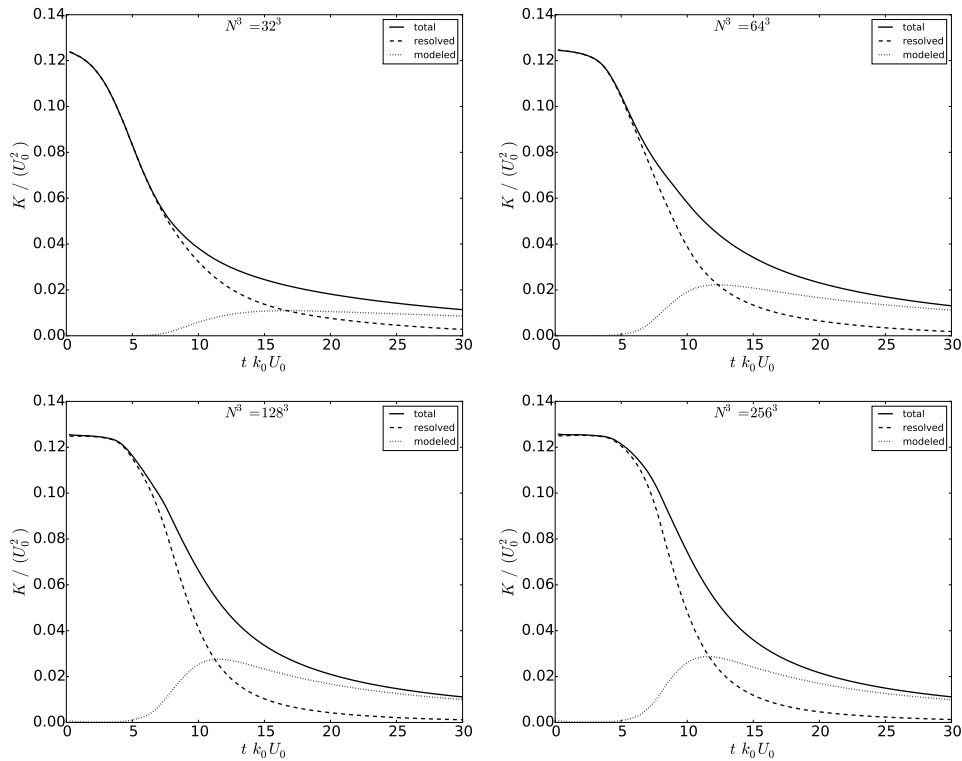


Figure 4: Total (solid), resolved (dashed) and modeled (dotted) kinetic energy (scaled) for the TGV simulation at with three meshes: $N^3 = 32^3$, 64^3 and 128^3 , as indicated.

energy is set to $K_o = 1 \times 10^5 \text{ cm}^2/\text{s}^2 \sim 1\%$ of the peak initial K .

In Figure (4) we show the decomposition of turbulent kinetic energy from (27). For all resolutions, before the onset of turbulence ($t^* = tk_0U_0 < 5$), the total TKE is dominated by the resolved TKE of the 4 vortices prescribed by the initial conditions. As turbulence develops and enstrophy peaks at $t^* \sim tk_0U_0 \sim 9$, when small scale structures start forming in Figure 3, the resolved TKE becomes smaller and the modeled TKE becomes larger. After the enstrophy has peaked, at times $t^* = tk_0U_0$ roughly between 9 and 15, we expect that, at the lowest resolution, the modeled TKE will constitute a larger fraction of the total TKE than the resolved TKE, while at the highest resolution, the modeled TKE would constitute a smaller fraction of the total TKE. However, we observe that the modeled TKE becomes larger as resolution increases, while the resolved TKE remains roughly unaffected by resolution. At later times, the total TKE is dominated by the modeled TKE, as the resolved TKE approaches zero, irrespective of the resolution we consider here. Thus, the hybrid formulation would seem to be behaving in the opposite way to what we expect. Indeed, we observe that at a given point in space and time, the contribution function f is larger at the higher resolution simulations (not shown here).

In Figure (5), we show corresponding decompositions for the TGV kinetic energy dissipation $-dK^*/dt^*$, and for reference, we show the available DNS predictions for the latter. For the finest resolution considered, 256^3 , the resolved dissipation overpredicts the DNS and peaks somewhat earlier than $t^* \sim tk_0U_0 \sim 9$, whereas the total dissipation is consistent with an LES *emulating* the Re=1600 DNS case. Likewise, we could argue that the total dissipation for the 128^3 and 64^3 cases approximately *emulate* the Re=800 and Re=400 DNS results, respectively, so that the grid-dependent LES generated with the hybrid strategy appears to behave similarly to the noted ILES behavior [33, 37] near transition time $t^* \sim tk_0U_0 \sim 9$ – as function of an effective Re increasing with resolution – when compared to the DNS. The results for the coarsest resolution, 32^3 cannot be explained in this fashion.

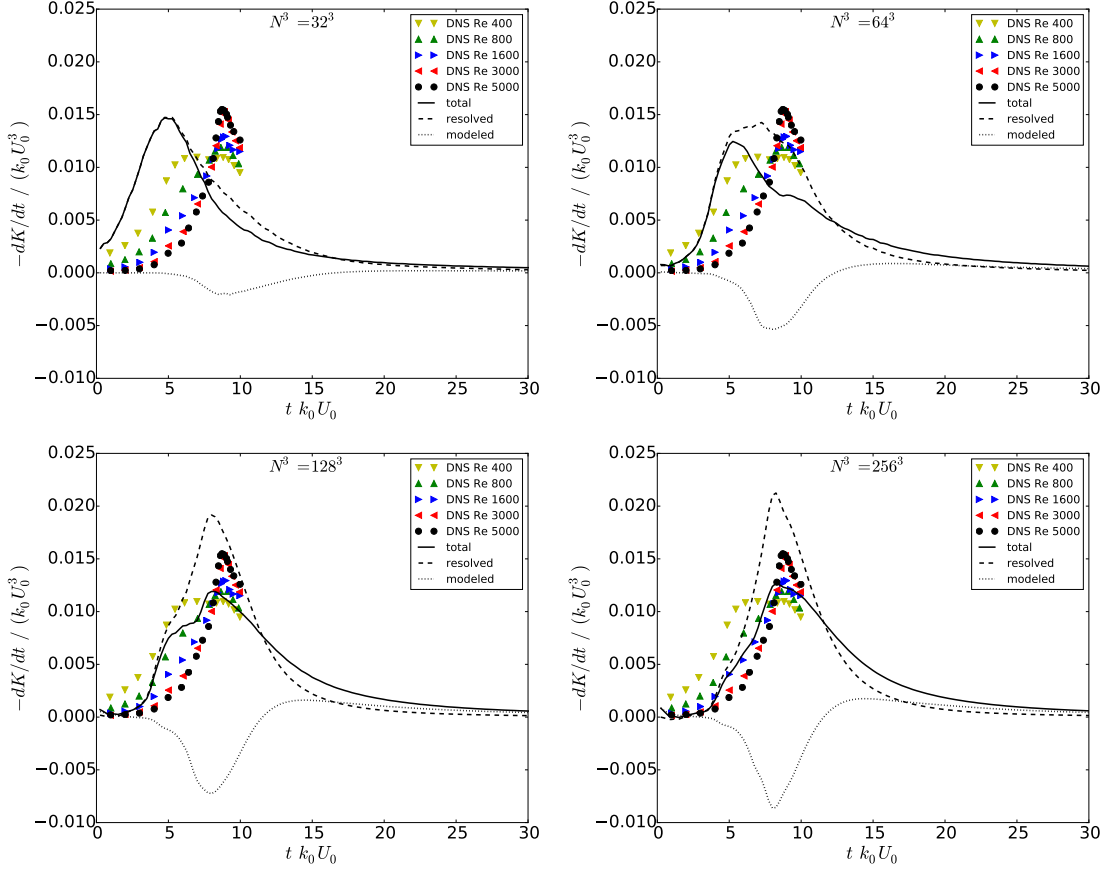


Figure 5: Total, resolved and modeled rate of dissipation of kinetic energy (scaled) for the TGV simulation at with meshes: $N^3 = 32^3$, 64^3 , 128^3 , and 256^3 as indicated. Results from available DNS [31, 32] at various different available Reynolds numbers are shown for reference.

7 Planar Shock Tube

We simulate a planar air/SF₆ shock-tube configuration that has been investigated previously in [6]. We use a domain of size $L_x = 80$ cm, $L_y = L_z = L = 24$ cm, in which low (air) and high (SF₆) density gases, with densities of 1.184×10^3 g/cm³ and 6.34×10^3 g/cm³, respectively, are separated by a perturbed interface located at $x = 20$ cm. The initial Atwood number of the flow is $A_t = 0.7$. The contact discontinuity between air and SF₆ is initially at rest, and is modeled as a jump in density using ideal gases with $\gamma = 1.4$ and $\gamma = 1.076$, respectively, with constant pressure. A shocked air region is created at $x \leq 15$ cm, upstream of the interface, satisfying the Rankine-Hugoniot relations for a Mach 1.5 shock. The shock propagates in the x direction through the contact discontinuity (from the light to heavy fluid). The simulations considered here stop before the shock is reflected off the right boundary. Periodic boundary conditions are imposed in the transverse (y, z) directions. The evolution and interaction of the shock and air/SF₆ interface are in good agreement with those of similar reported studies.

Because shocks and turbulence are involved, resolving all relevant physical scales in shock-driven turbulence simulations becomes prohibitively expensive. ILES addresses the difficult issues posed by under-resolution, by relying on SGS models provided implicitly by physics capturing numerics, providing an effective strategy combining shock and turbulence emulation capabilities based on a single numerical model. The surface displacement of the material interface in shock-tube experiments has been typically modeled using superimposed well-defined spectral modes often combined with random perturbation components. The

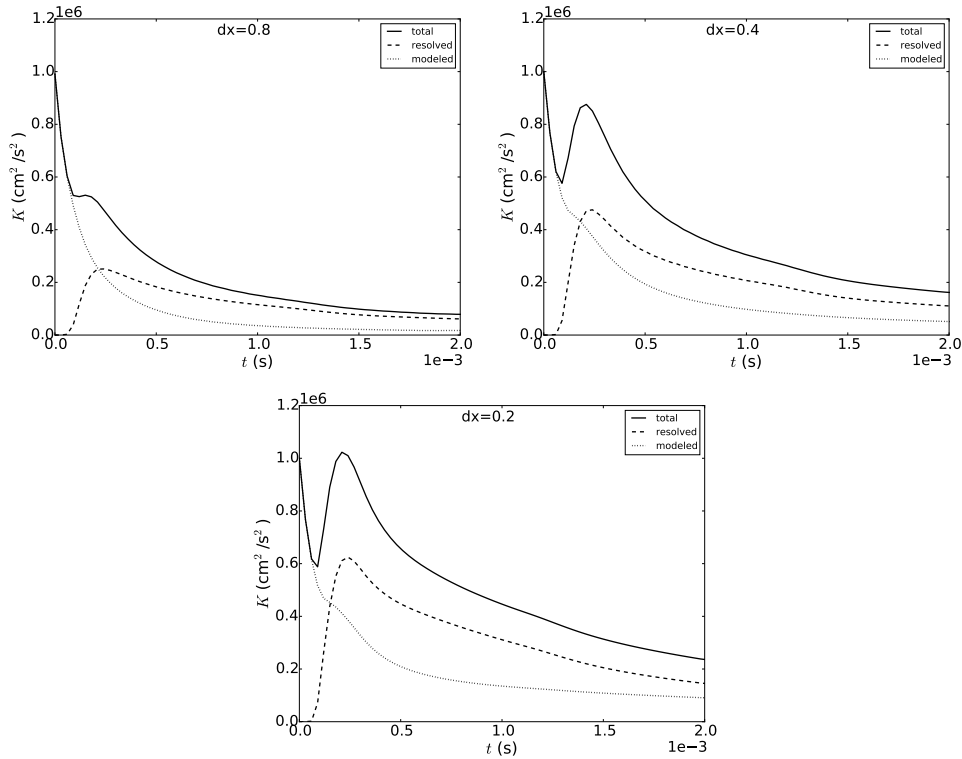


Figure 6: Total, resolved and modeled kinetic energy for the air-SF₆ shocktube problem at three resolutions, as indicated. The initial BHR length scale is fixed at $S_o = 0.1$ cm for all simulations.

interface perturbation ψ is defined using a random spectral representation,

$$\psi = \sum (A_i \cos(2\pi/L_y(m_i y + r_{yi})) \cos(2\pi/L_z(n_i y + r_{zi}))) \quad (31)$$

where

$$A_i = \Gamma \left(\sqrt{m_i^2 + n_i^2} \right)^s, \quad (32)$$

for $i = 1, \dots, N$, where N is the number of modes used, Γ is chosen so that standard deviation of ψ is equal to the prescribed standard deviation $s.d. = 1.0$ cm. The perturbation amplitude has a slope $s = -2$ in spectral space. The wavenumbers are chosen such that $4 \leq k \leq 12$ with $k = \sqrt{k_m^2 + k_n^2}$, $k_m = 2\pi m/L$, $k_n = 2\pi n/L$, resulting in $N = 108$ modes.

For the TGV case above, long wavelengths (compared to grid size) are initially involved and smallest generated length scales are constrained by grid size, so that choosing a variable initial turbulent length scale in BHR $S_o = \Delta$ appears meaningful. In contrast, for the shock-tube case, it is natural that S_o be fixed – as IC characteristic, and that S_o and $s.d.$ should be related (e.g., proportional) given that larger interface perturbations are capable of producing more turbulent flows and S_o is inversely proportional to the TKE decay rate in the BHR equations. For historical reasons, $S_o = 0.1$ cm. was chosen in the current shock-tube hybrid implementation.

We run simulations with the hybrid scheme using three uniform resolution meshes, with $\Delta = 0.2, 0.4$ and 0.8 cm, respectively. The BHR initial specific turbulent kinetic energy is set at $K_o = 1 \times 10^6$ cm²/s², based on independent, high resolution ILES using an adaptive refinement mesh with 5 levels, with $\Delta = 0.05$ cm at the highest resolution level. For each simulation, we diagnose the TKE decomposition in equation (27), shown in Figure (6). The shock goes over the interface at about $t = 1.2 \times 10^{-4}$ s, after which Richtmyer-Meshkov instability ensues in the proximity of the material interface, generating a mixing layer. The TKE of the flow peaks at about $t = 2.5 \times 10^{-4}$ s, after which it decays. As resolution increases, the total TKE increases, and

this increase is mainly dominated by increasing resolved TKE, as in the TGV flow simulations. Again, the increase of modeled TKE with increasing resolution is associated to an increase in the dynamic contribution function with increased resolution within the mixing region at any point in time (not shown here) – whereas both should decrease as resolution increases.

8 Discussion

We proposed a dynamic blended hybrid RANS/ILES strategy, and report progress testing its preliminary implementation for relevant canonical problems involving unsteady variable-density turbulent flows. The hybrid approach considered here is based on the FSM [18, 14], locally blending a high resolution computational strategy with RANS modeling – depending on how much of the turbulence is resolved at given resolution, and providing a sophisticated CGS strategy in-between. How much dissipation is modeled and how much is computed is decided based on having the RANS model locally morph into a CGS SGS model, in terms of contribution function $f : 0 < f < 1$. Here, at the high resolution limit $f = 0$, involving ILES, and at the low resolution limit $f = 1$, producing a pure RANS closure. We use a strategy proposed by Germano [15, 16] to generate f dynamically, by using an identity that relates total, unresolved and resolved stresses, an implicit grid filter as the primary filtering operation and a differential filter as the secondary filtering operation. In contrast with explicit dependence of the contribution function f on grid size in the classical blended hybrids, the approach we use here results in an implicit dependence of f on grid size.

We tested the dynamic contribution function by using the hybrid RANS/LES formulation to simulate two representative flows of interest. For each case we used three or four different resolutions in order to verify whether the hybrid RANS/LES simulations behaved as expected. In particular, the contribution function f and the modeled turbulent kinetic energy should be largest in the coarsest resolution simulations, where the simulation should rely more on BHR, the RANS model. However, we observe the opposite, that the contribution function f and the modeled turbulent kinetic energy are smallest in the coarsest resolution simulations, and they are largest at the finest resolution simulations, thus indicating that the latter simulations rely more on BHR. We speculate that this shortcoming is due to the RANS model, BHR, being operating on an eddying flow regime – for which it is not designed – thus encountering large density gradients and consequently producing excessive TKE and too high Reynolds stresses. This makes the denominator of the second term on the right hand side of equation (25) larger, leading to larger f . A larger f in the momentum equation (3) leads to more energetic flow, which leads to larger gradients, thus producing a feedback on f that prevents it from decreasing to smaller values.

Shortcomings of this preliminary implementation of our dynamic blended hybrid reflect on the need to further constrain the contribution function f to ensure that the RANS BHR terms scaled by f – i.e. the generated CGS SGS model terms, are themselves physically consistent. This is not needed when proper behaviors at the coarse and fine resolution limits are enforced through f being *explicitly* defined in terms of local grid size Δ . To address this issue, we plan to explore averaging the prognostic variables along directions of homogeneity in space and/or time before they are used to compute the BHR closure equations, so that effectively the RANS model operates on mean flow quantities. Further, we will examine the terms in the Germano decomposition in high resolution simulations to verify that it is plausible to obtain a dynamic contribution function with expected behaviors from our formulation.

Acknowledgements

We thank Massimo Germano for many insightful discussions and comments. Los Alamos National Laboratory is operated by LANS, LLC for U.S. DOE NNSA under Contract No. DE-AC52-06NA25396.

References

- [1] Grinstein, F.F., Coarse Grained Simulation and Turbulent Mixing, Cambridge, 2016.
- [2] Zhou, Y., Grinstein, F.F., Wachtor, A.J. & Haines, B.M., Estimating the effective Reynolds number in implicit large-eddy simulation, Phys. Rev. E, 89, 013303, 2014.

- [3] Grinstein, F.F., Margolin, L.G., & Rider, W.J., *Implicit Large Eddy Simulation: Computing Turbulent Flow Dynamics*, Cambridge UP, NY, 2nd printing, 2010.
- [4] Hirt, C.W., Computer studies of time-dependent turbulent flows, *Phys. Fl. Suppl. II*, pp. 219-227, 1969.
- [5] Ghosal, S., An analysis of numerical errors in large-eddy simulations of turbulence, *J. Comput. Phys.*, 125, 187-206, 1996.
- [6] Ristorcelli, J. R., Gowardhan, A.A. & Grinstein, F.F., Two classes of Richtmyer-Meshkov Instabilities; a detailed statistical look, *Physics of Fluids*, 25, 044106, 2013.
- [7] Frolich J & von Terzi, D.A., Hybrid LES/RANS methods for the simulation of turbulent flows, *Progress in Aerospace Sciences*, 44, 349-77, 2008.
- [8] George, W.K. & Davidson, L., Role of Initial Conditions in Establishing Asymptotic Flow Behavior, *AIAA Journal*, 42, 438-446 (2004).
- [9] Grinstein, F.F., Initial Conditions and Modeling For Simulations of Shock Driven Turbulent Material Mixing, *Computers and Fluids*, 151, 58-72, 2017.
- [10] Poggi, F., Thorembey, M-H. & Rodriguez, G., Velocity measurements in turbulent gaseous mixtures induced by Richtmyer-Meshkov instability, *Physics of Fluids*, 10, 2698, 1998.
- [11] Gittings, M., Weaver, R., Clover, M., Betlach, T., Byrne, N., Coker, R., Dendy, E., Hueckstaedt, R., New, K., Oakes, W.R, Ranta, D., Stefan, R., The RAGE radiation hydrodynamic code, *Comput. Science & Discovery* 1, 015005, 2008.
- [12] Hahn, M., Drikakis, D. L. Youngs, & R. J. R. Williams, Richtmyer-Meshkov turbulent mixing arising from an inclined material interface with realistic surface perturbations and reshocked flow, *Phys. Fluids*, 23, 046101, 2011.
- [13] Haines, B.M., Grinstein, F.F. & Schwarzkopf, J.D., Reynolds-averaged Navier-Stokes initialization and benchmarking in shock-driven turbulent mixing, *Journal of Turbulence*, 14:2, 46-70, 2013.
- [14] Fasel, H.F., von Terzi, D.A. & Sandberg, R.D., A Methodology for Simulating Compressible Turbulent Flows, *J. Appl. Mech.*, 73, 405-412, 2006.
- [15] Germano, M., Readers' forum, Comment on Turbulence Modeling for Time-Dependent RANS and VLES: A Review, *AIAA Journal*, 36(9), 1766-1767, 1998.
- [16] M. Germano. Differential filters for the large eddy numerical simulation of turbulent flows. *The Physics of Fluids*, 29(6):1755-1757, 1986.
- [17] Spalart, P.R., Detached-eddy simulation, *Annu. Rev. Fluid Mech.* 41, 181–202, 2009.
- [18] Speziale, C.G., 1998, A Combined Large-Eddy Simulation and Time-Dependent RANS Capability for High-Speed Compressible Flows, *J. Sci. Comput.*, 13, pp. 253–274.
- [19] M.Y. Hussaini, S. Thangam, S.L. Woodruff, Y. Zhou , Development of a Continuous Model for Simulation of Turbulent Flows, *Journal of Applied Mechanics*, 73, 441, 2006.
- [20] L.J. Peltier, F.J. Zajaczkowski, Maintenance of the near-wall cycle of turbulence for hybrid RANS/LES of fully-developed channel flow, in *DNS/LES Progress and Challenges*, Proc. of the 3rd AFOSR International Conference on DNS/LES, ADP013707, Kluwer Academic (2001).
- [21] Girimaji, S.S., Partially-averaged Navier-Stokes model for turbulence: a Reynolds-averaged Navier-Stokes to direct numerical simulation bridging method, *Journal of Applied Mechanics*, 2006, 73, 413-421.
- [22] M. Germano. A statistical formulation of the dynamic model. *Physics of Fluids*, 8(2): 565-570, 1996.
- [23] Bose, S.T., Moin, P. & You, D. 2010, Grid-independent large-eddy simulation using explicit filtering, *Phys. Fluids*, 22, 1-11.

- [24] Hill, D.J., Pantano, C. & Pullin, D.I. 2006, Large-Eddy Simulation and Multiscale Modeling of a Richtmyer-Meshkov Instability with Reshock, *J. Fluid Mech.*, 557, 29-61.
- [25] Besnard, D., Harlow, F.H., Rauenzahn, R.M., and Zemach, C., Turbulence transport equations for variable-density turbulence and their relationship to two-field models, LA-UR- 12303, Los Alamos National Laboratory, 1992.
- [26] Schwarzkopf, J.D., Livescu, D., Gore, R.A., Rauenzahn, R.M., Ristorcelli, J.R., Application of a second-moment closure model to mixing processes involving multi-component miscible fluids, *Journal of Turbulence*, 12, No. 49, pp. 1-35, 2011.
- [27] J. D. Schwarzkopf, D. Livescu, J. R. Baltzer, R. A. Gore, J. R. Ristorcelli, A two-length scale turbulence model for single-phase multi-fluid mixing, *Flow Turbulence Combust*, 96:1-43, 2016.
- [28] Walters, D. K., et al., Investigation of a Dynamic Hybrid RANS/LES Modeling Methodology for Finite-Volume CFD Simulations, *Flow, Turbulence and Combustion*, 91(3), 643-667, 2013.
- [29] S. Bhushan and D. K. Walters. A dynamic hybrid reynolds-averaged navier-stokes large eddy simulation modeling framework. *Physics of Fluids*, 24(1):015103, 2012.
- [30] J. R. Bull, M. D. Piggot, and C. C. Pain. A finite element les methodology for anisotropic inhomogeneous meshes. In THMT-12. Proceedings of the Seventh International Symposium On Turbulence, Heat and Mass Transfer, pp. 1516-1527, 2012.
- [31] Brachet, M.E., Meiron, D.I., Orszag, S.A., Nickel, B.G., Morg, R.H. and Frisch, U.J., Small-scale structure of the Taylor-Green vortex, *J. Fluid Mech.* 130, 411, 1983.
- [32] Brachet, M.E., Direct numerical simulation of three-dimensional turbulence in the Taylor-Green vortex, *Fluid Dynamics Research*, 8, 1, 1991.
- [33] Drikakis, D., Fureby, C., Grinstein, F.F., and Youngs, D., Simulation of transition and turbulence decay in the Taylor-Green Vortex, *Journal of Turbulence*, 8, 020, 2007.
- [34] Jeong, J. and Hussain, F., On the identification of a vortex, *J. Fluid Mech.* 285 69–94, 1995.
- [35] Frisch, U., *Turbulence*, Cambridge University Press, Cambridge, UK (1998).
- [36] Shu, C-W., Don, W-S., Gottlieb, D. Schilling, O. & Jameson, L. 2005, Numerical Convergence Study of Nearly Incompressible, Inviscid Taylor-Green Vortex Flow, *Journal of Scientific Computing*, 24, pp. 1-27.
- [37] Grinstein, F.F., A.A. Gowardhan, and A.J. Wachtor, Simulations of Richtmyer-Meshkov instabilities in planar shock-tube experiments, *Phys. Fluids* 23, 034106, 2011.